Publisher version: doi: 10.1061/(ASCE)HY.1943-7900.0001212

Preprint of Capape, S., Martín-Vide, J., and Colombo, F. (2016). "Subaqueous Barchans and Plane Beds from Deposition of Quartz Silt." *J. Hydraul. Eng.*, 10.1061/(ASCE)HY.1943-7900.0001212, 06016020

Subaqueous Barchans and Plane Beds from Deposition of Quartz Silt

S. Capape[1]*, J.P. Martín-Vide[2], and F. Colombo[3]

Abstract

The suspension flow of quartz silt (geometric mean grain size of 4.15 microns), in unfavourable conditions for the deposition, originates the development of different bed morphologies. Particles deposit over a plane, non-erodible surface and develop well-defined barchan ripples, barchanoids and plane beds in flume experiments. Bed-load transport of quartz silt by bedform migration is several orders of magnitude smaller than the suspended transport. The final bed morphology is controlled by the suspended sediment concentration and the running time of the experiment. The average dimensions of the bedforms after one-day experiments are 4.93 cm wide, 10.33 cm long and 0.45 cm high. Cohesive plane beds appear after two and three-days experiments with very high sediment concentration ($\geq$ 22.5 kg/m^3). Viscous effects are deemed relevant for the formation of the beds. DOI: 10.1061/(ASCE)HY.1943-7900.0001212. © 2016 American Society of Civil Engineers.

[1] Ph.D Student, Technical University of Catalonia-BarcelonaTech, Barcelona, Catalonia.
*Corresponding author c/ Jordi Girona 1, D1-204, 08034 Barcelona, Catalonia, Spain. E-mail: sergi.capape@upc.edu
[2] Professor, Technical University of Catalonia-BarcelonaTech, 08034, Barcelona, Catalonia, Spain
[3] Professor, SIMGEO UB-CSIC, Departament d'Estratigrafia, Paleontologia i Geociències Marines, Universitat de Barcelona, 08028, Barcelona, Catalonia, Spain
Note. This manuscript was submitted on September 7, 2015; approved on May 24, 2016; published online on August 3, 2016. Discussion period open until January 3, 2017; separate discussions must be submitted for individual papers. This technical note is part of the Journal of Hydraulic Engineering, © ASCE, ISSN 0733-9429.

Introduction

Common knowledge points to conditions for a significant sediment suspension when the shear velocity is much larger than the settling velocity of the particles (Bagnold 1966). The flow properties, the sediment concentration, the particle size distribution and the cohesive attributes affect the deposition of the particles (Baas et al. 2011; Jopling and Forbes 1979). In the experiments reported here, although the shear velocity was considerably larger than the settling velocity of the particles, multiple bed morphologies developed from the deposition of quartz silt (geometric mean grain size of 4.15 μm) over a plane, rigid, non-erodible surface in turbulent conditions. In this article, the authors show evidence for the bed formation, with few examples in the literature (e.g. Jopling and Forbes (1979)).

An extensive catalogue of bedforms can emerge on the bed from the interaction between the flow and the bed material (Allen 1968) although a noncohesive sediment with a median smaller than 150 μm confines the possibilities of bedforms to ripples (Southard and Boguchwal 1990). Ripples may be defined as small bedforms independent of flow depth but dependent of the grain size distribution that scale with the thickness of the viscous sublayer (Jopling and Forbes 1979; Mantz 1992). Over time, the ripples grow and evolve towards an equilibrium 3D linguoid shape (Baas 1994, 1999; Mantz 1992; Raudkivi 1997). When the ultimate equilibrium bed displays no linguoid geometries in plan, it is interpreted as a lack of equilibrium because either there has been insufficient time to develop the geometry or there is a deficit of supply of noncohesive granular material (Baas et al. 2013). The equilibrium bedform sequence from a stationary flat bed shows barchanoid ripples followed by linguoid ripples with increasing flow discharge (Mantz 1992). Linguoid ripples have short, strongly curved open out upcurrent crestlines, as opposed to barchanoids whose crestlines open out downcurrent (Allen 1968).

Barchan ripples are bedforms related to sediment transport at below-capacity conditions (Mantz 1978), with geometry in plan of crescent moon (which explains the *lunate* terminology) and two horns pointing towards the dominant flow direction. Subaqueous barchans have been reported in fluvial (McCulloch and Janda 1964), marine (Hollister and McCave 1984) and estuarine (Allen 1968) environments, in laboratory experiments (Courrech du Pont et al. 2014; Endo et al. 2005; Franklin and Charru 2011; Groh et al. 2009; Hersen 2005; Hersen et al. 2002; Katsuki et al. 2005; Mantz 1978) and in industry (Boulanger and Wong 2016). Barchanoid-type bedforms comprise not only isolated barchans but also parallel rows of coalesced barchans (McKee 1980), simply called barchanoids, which may precede the barchan formation (Endo et al. 2005). The observations from linear stability analysis on aeolian sand barchans are that barchan corridors are unstable (although actual barchan corridors do not manifest such instabilities) (Hersen et al. 2004) and that barchans can be formed from transverse dunes moving on a non-erodible bed (Melo et al. 2012; Parteli et al. 2011).

Method

Experimental apparatus and sediment description

The experiments are performed in a rectangular tilting flume (Laboratory of Geological Processes Simulation SIMGEO UB-CSIC, Universitat de Barcelona) 15 m long, 0.37 m wide and 0.40 m high. The floor consists of rigid polished aluminium and the walls are transparent glass. The water and sediment mixture is constantly recirculated (Fig. 1) on the principle of mass conservation (i.e. the sediment can only deposit on the bottom of the flume as the mixture is stirred in the rest of the facility). Velocity is measured using the acoustic Doppler principle, water level is measured using point gauges, and sediment concentration is obtained from oven-drying samples of mixture at

different elevations. The temperature is also monitored. Direct town supply, drinking water is used (salinity, pH and total hardness are 500 mg/l, 7.5 and 260 mg $CaCO_3$, respectively).

The sediment is made of crushed rock and consists of SiO_2 (quartz >97%) and traces of Al_2O_3, K_2O, CaO, Fe_2O_3 and TiO_2. The geometric mean size D_g = 4.15 μm and the geometric standard deviation σ_g = 2.38 [Fig. 2(a)]. It is poorly sorted (Folk 1974) and noncohesive by definition although beds made of this material may behave as cohesive (Roberts et al. 1998; te Slaa et al. 2015; Walder 2015). The settling velocity is obtained from Stokes' solution $w_s = g \cdot R \cdot D^2/(18 \cdot \nu)$ valid for very small particles (Graf 1984), with g = 9.81 m/s^2 the acceleration of gravity, R = 1.6 the submerged specific gravity of sediment (density of the silt ρ_s = 2600 kg/m^3), $\nu = 0.77 \cdot 10^{-6}$ m^2/s the mean water kinematic viscosity and D a grain size. The settling velocities for the characteristic grain sizes D_g, D_{10} = 1.25 μm and D_{90} = 12.48 μm are $1.95 \cdot 10^{-5}$ m/s, $1.77 \cdot 10^{-6}$ m/s, and $1.76 \cdot 10^{-4}$ m/s, respectively. The high resolution image in Fig. 2(b) shows particles with sharp edges and a size range comprising from < 1 μm to ~10 μm.

Procedure

Quartz silt and 4.8 m^3 of water are first mixed within the tank and then pumped (the aspect is that of a dense milk). The stirring within the tank is never stopped. The initial conditions are always the rigid, non-erodible clean floor of the flume but the initial sediment concentrations are varied with a maximum of 51.72 kg/m^3 as described in Table 1. The experiment starts after flow of water and sediment is stabilized (Fig. 1) and runs continuously, with the hydraulic conditions constant and without adding silt. At the end of the run the pump is turned off and the remaining water and silt in suspension slowly evacuate the flume by gravity without modifying the bedforms. A trivial quantity of silt may deposit during the emptying of the flume.

Photographs of the new bed are taken and processed to obtain mean sizes of the bedforms (length and width). Bed thicknesses are measured with a point gauge and the laser diffraction technique is used to obtain grain size distributions from samples of deposited silt.

The 12 experiments are classified in 3 groups based on their duration t: 1) short experiments (t = 100 min); 2) one-day experiments (t = 1440 min) and 3) long experiments ($t \geq 2040$ min). The bedform development and equilibrium hypotheses are tested by studying the different bed morphologies at the end of the runs. The beds of silt constitute, on average, 10%, 33% and 41% of the initial silt in suspension in group 1, 2 and 3, respectively [Table 1].

The discharge is evaluated as $Q = U \cdot B \cdot h = 7.7 \cdot 10^{-3}$ m^3/s, where $U = 0.27$ m/s is the depth-averaged velocity and $h = 0.077$ m is the flow depth. The flume bed slope is $S_b = 6 \cdot 10^{-4}$ and the energy gradient is $S_f = 4.8 \cdot 10^{-4}$ from water level readings 10.7 m apart. The Reynolds number $\mathrm{Re} = 4 \cdot R_h \cdot U / \nu = 7.5 \cdot 10^4$, where R_h is the hydraulic radius, defines a turbulent flow, and the Froude number $\mathrm{Fr} = U / \sqrt{(g \cdot h)} = 0.31$ defines a subcritical flow. The average shear velocity is approximated as $u_* \approx \sqrt{(g \cdot R_h \cdot S_f)} = 0.016$ m/s (~90 times bigger than the settling velocity of a particle of size D_{90}). The Chezy's resistance coefficient $C_z = U/u_*$ is used to compute the equivalent bed roughness k_s from the Colebrook and White relation (Henderson 1966), given as:

$$\frac{C_z}{\sqrt{8}} = -2 \cdot \log_{10}\left(\frac{k_s}{12 \cdot R_h} + \frac{2.5 \cdot C_z}{\mathrm{Re} \cdot \sqrt{8}}\right) \qquad [1]$$

leading to $k_s = 6.0 \cdot 10^{-4}$ m (~50 times bigger than the quartz silt size D_{90}). The viscous sublayer is defined as $\delta_v = 11.6 \cdot \nu / u_* = 5.6 \cdot 10^{-4}$ m so $0.25 < k_s/\delta_v < 6.0$ and the bed is hydraulically in transition (Cardoso 1998).

Results and discussion

Regardless of the initial suspended sediment concentration, silt accumulations appear at the end of our experiments as shown in Fig. 3 and Table 1. Mass deposition (Mehta 2013) is excluded based on observations and the noncohesive character of the quartz silt. From E1 to E12 in Fig. 3, the beds of quartz silt show an early stage of bed formation, evolve into barchans for the one-day experiments and flatten into cohesive plane beds for the long experiments. Overall, the sequence in Fig. 3 from group 1 (t = 100 min) to group 3 ($t \geq 2$ days) may reveal stages of the formation of an equilibrium fine sediment bed from particle sedimentation. The deposition of silt occurs at a faster rate during the first minutes (Fig. 4). The amount of deposited silt agrees with the decrease of the suspended silt concentration. The measured wet and dry bulk density of the bed is 1820 and 1340 kg/m^3, respectively, which agrees with the values obtained in previous research with quartz silt (Roberts et al. 1998; te Slaa et al. 2015). During the initial stage of the runs, with a faster deposition rate, multiple small and *coarse* bedforms are created 8Fig. 3) but, over time, there are changes in the bed morphology as a consequence of bedform migration and interactions and further sedimentation of finer particles.

Group 1

The group 1 (E1 and E2 in Fig. 3) displays similar beds although initial silt concentration in E2 (21.30 kg/m^3) is nearly three times the silt concentration in E1 (7.51 kg/m^3). The bed morphology is defined as barchanoids because many of the bedforms appear in contact to each other. Following Allen (1968), some 2D features are assigned to these bedforms because they are comparatively much wider than higher ($W \sim 13 \cdot H$ as given in Table 1); then, a crestline may be drawn to span the whole width of the flume. Subsequently, bedforms are grouped in horizontal bands, perpendicular to the main flow direction. It is termed barchan front [Fig. 5(a)].

Sidewall effects are clear in group 1, approximately up to a fifth of the total width from the sidewall. Indeed, bedforms near the wall appear behind the rest of the bedforms of the barchan front, a feature which may correspond to an initial state of the bedforms (Baas 1994).

In group 1 runs, 6.5 cm long barchanoids are 3 cm shorter approximately than the rest of the experiments bedforms. The width and height, 4.8 cm and 0.5 cm respectively, are similar to the rest of the experiment measures. The distance between two consecutive barchan fronts λ is ~9.1 cm. A length λ is also defined in E9 and E10.

Group 2

The initial silt concentration ranges between 1.3 kg/m^3 and 9.8 kg/m^3 and all experiments last one day. In these quartz silt beds the barchans are discernible on the bottom of the flume. Specially E3 (Fig. 3) displays similarities with other research focused in the creation of barchans (e.g. Endo et al. (2005)). The rear-point of the barchan is unclear when it resembles a comet [Fig. 5(b)] so, in these cases, the length of the barchan L does not include the tail. The cohesive-like behaviour of the silt bed may explain the ripple elongation (Schieber et al. 2013).

A horn length L_h is defined for all experiments with barchanoid morphology in spite of the difficulty of interacting bedforms and the asymmetry. The average total length of the bedforms in group 2 (i.e. the sum of the barchan length and the horn length) is 11.73 cm. On average, bedforms are 4.93 cm wide, 10.33 cm long and 0.45 cm high and have horns 1.40 cm long. The angle between the lee-side and the floor of the flume is 20.1º in average, smaller than the ~30º typically seen for ripples (Allen 1968) and aeolian-dominated sandy material in desert barchans (Sauermann et al. 2000), although low-angle lee-side dunes (< 10º) are also common (Best 2005).

148 The barchans in group 2 have ratios L_h/W and L/W greater than 0.21 and 1.9, respectively. The
149 former is slightly lower than 0.35 reported for barchans in unidirectional water flows (Endo et al.
150 2005).
151 The biggest bedforms appear for experiments with higher initial suspended silt [Table 1], with
152 barchans up to 0.69 cm high. Following Fig. 3, the average volume of a barchan grows [E3-E5],
153 shrinks [E6-E7] and ultimately grows [E8-E10], and the silt plane layer of thickness s [Fig. 5(c)]
154 grows [E3-E8] and then shrinks [E9-E10]. This points to a competition between the barchan
155 formation and the deposition of particles as a plane layer.
156 The interactions between barchans are more noticeable for experiments with higher sediment
157 concentration. The processes of absorption, ejection and split taking place on the bottom of the
158 flume are suspected (Endo et al. 2004) and they may explain the decrease in the number of
159 bedforms from group 1 to group 2 observed in Table 1. The runs E9 and E10 have similar sediment
160 concentration and both have bigger bedforms than the rest on group 2. The bedforms in E9 and
161 E10 are touching each other, with merging horns, and they may resemble a barchan front. Between
162 consecutive barchans the floor of the flume may be visible.
163 The sidewall effects are not as clear on this group. Attached to the walls there are *halved* bedforms
164 in agreement with the moving bedforms that a viewer can see from the side of the flume, during
165 the experiments, and whose velocity can be measured as reported later.
166 *Group 3*
167 The beds of maximum thickness s are obtained after experiments lasting 3 days (E11) and 2 days
168 (E12) with very high sediment concentration [Table 1]. Surprisingly, the morphology of these beds
169 is totally different from the rest of the experiments because the silt creates a plane layer, slightly
170 concave (the sides are thicker than the middle of the bed), that covers the whole length of the flume

where bedforms have vanished. It is possible to spot few bedforms in the middle of the cross-section, covering 1/3 of the total width. The accumulation on the sides in E12 is up to 2.26 cm thick.

The plane beds in group 3 are presumably preceded by bedforms under the assumption that final quartz silt beds formed in short experiments (e.g. E2) are also the quartz silt beds existing at an intermediate time in long experiments (e.g. E11). As Andreotti et al. (2002) show that a flat bed is unstable at large wavelengths from linear stability analysis, cohesion should play a role in the plane bed observed in runs E11 and E12.

Migration rate and bed-load

The suspended quartz silt only allowed the visualization of migrating bedforms on the sidewall of the flume, where they are altered by the presence of the wall (Fig. 3). The incipient bedforms (with height less than ~3 mm) migrate at ~4 mm/min, and over time they grow and migrate slower, at ~1 mm/min. As it is frequently reported, the migration rate and bedform height are inversely proportional (Endo et al. 2004; Hersen 2005; Hersen et al. 2002; Simons et al. 1965). These migration rates agree with the values from Hersen (2005) (using glass beads of 150 μm), but are comparatively ~80 times smaller than the values from Endo et al. (2005) (using a mean particle size of 100 μm). The reader should keep in mind that the quartz silt in the present experiments is much smaller than the sediment size reported in the previous studies.

The velocity of the bedforms $V_s \approx 1$ mm/min is used to compute the observed bed-load transport with the expression from Simons et al. (1965) for a regular sequence of triangular bedforms, migrating without deforming, given as:

$$Q_{b,o} = N \cdot \frac{H}{2} \cdot B \cdot (1 - p) \cdot V_s \qquad [2]$$

where $Q_{b,o}$ is the observed bed-load transport in m^3/s, H and N are respectively the mean height of the bedforms and the ratio of area of flume bottom with barchans to total area of flume bottom given in Table 1, $B = 0.37$ m is the flume width, and $p = 0.48$ is the measured porosity of the bed of silt. Then, the average observed bed-load is $Q_{b,o} = 2.06 \cdot 10^{-9}$ m^3/s (without considering the plane layer of silt that sometimes covers the flume) and is some orders of magnitude smaller than the suspended sediment transport (e.g. the suspended sediment transport is $3 \cdot 10^{-6}$ m^3/s if the suspended sediment concentration is 1 kg/m^3).

The bed-load is also evaluated with the transport equation from van Rijn (1984) —although it should be used for sediment sizes > 200 μm— given as:

$$Q_{b,c} = 0.053 \cdot B \cdot D \cdot \sqrt{g \cdot R \cdot D} \cdot \frac{T^{2.1}}{D_*^{0.3}} \qquad [3]$$

where $Q_{b,c}$ is the computed bed-load transport in m^3/s, D is the bed particle size from Table 2, $T = (u_*^2 - u_{*c}^2)/u_{*c}^2$ with u_{*c} the critical shear velocity for initiation of motion and $D_* = D \cdot (R \cdot g/\nu^2)^{1/3}$. The formula is computed for one particle size of 10 μm and two values for the critical shear velocity from van Rijn (2007): for noncohesive pure quartz grains $u_{*c} = 0.006$ m/s and the bed-load is $Q_{b,c} = 1.94 \cdot 10^{-7}$ m^3/s; to account for cohesion effects on the bed $u_{*c} = 0.013$ m/s and the bed-load is $Q_{b,c} = 1.14 \cdot 10^{-9}$ m^3/s. Therefore, although multiple simplifications have been introduced, there is some agreement between the observed bed-load from only migrating bedforms and the bed-load obtained from the transport equation of van Rijn (1984), provided the critical shear velocity for initiation of motion is well defined.

Grain size

A reasonable assumption is that if a long experiment stops at the duration of the short experiment, the two beds will be the same. On average, the bed is 2.3 times coarser than the silt in the initial

suspended mixture in group 1 (short experiments) but is reduced to 1.6 times coarser in group 3 (long experiments) [Table 2]. Particularly, comparing the particle size distribution between beds from groups 1, 2 and 3, there is an excess of the volume fraction of particles ~13.6 μm in group 1 whereas the beds from groups 2 and 3 contain an excess of particles of ~5 μm.

The segregation of the particles during the bed formation relates to coarser fractions depositing earlier, so the deposition rate is faster during an early stage of the run (Fig. 4). From the poorly sorted silt in suspension (σ_g = 2.38), coarser particles may become trapped within the viscous sublayer whereas finer particles are preferentially rejected as suggested by McCave (1970, 2008).

Formation of the bed

As the bed remains hydraulically in transition condition ($k_s/\delta_v < 6$) (Cardoso 1998), particles entering the viscous sublayer may *a*) become trapped in the flume bed (McCave 2008); *b*) become trapped in the stoss-layer of a barchan (Zhang et al. 2014); *c*) become resuspended by the vortices originated in an upstream barchan (Endo et al. 2004); *d*) become resuspended because they are ejected from the horns of the barchan (Zhang et al. 2014); or *e*) become entrained into suspension by turbulent processes affecting the viscous sublayer (Niño et al. 2003). The aspects *c*) and *d*) do not imply that particles escape the viscous sublayer and all these processes may unfold the formation of fine sediment beds from a suspension.

As the threshold shear velocity of entrainment into suspension u_{*s} (from Niño et al. (2003) criterion) is greater than the estimated shear velocity for the experiments (e.g. if evaluated for a particle size of 10 μm, $u_{*s}/u_* \approx 1.3$), particles captured within the viscous sublayer may not escape. Therefore, viscous effects are twofold; first, they are probably responsible for the trapping of particles on the bed; and second, they prevent bed erosion.

From the previous ideas and the scrutiny of the beds in Fig. 3, particularly the sequence from E1 (group 1) to E3 (group 2), the bed formation is conjectured as: 1) particles are captured within the viscous sublayer; 2) captured particles form barchan ripples, indicators of sediment transport under below-capacity conditions (e.g. Mantz (1978)); 3) the supply of fine sediment to the viscous sublayer does not cease; and 4) the interaction between barchans induces the reduction of the number of barchans and its growth.

The transformation from group 2 bedform-covered floor to group 3 plane bed needs further research. Not only the silt concentration is the maximum on group 3, but also the experiments are the longest and the cohesive effects may be significant. It may involve the saturation of silt on the bed and a change to at-capacity conditions of the silt transport, so the first barchans to appear on the bed (e.g. E2 in group 1) cannot reshape the continuing deposition of particles. Also, viscous effects and their presumed protective action on the bed may limit the supply of particles for full bedform development (Baas et al. 2013). More detailed experimental analysis is required to test these hypotheses.

Concluding remarks

Quartz silt in suspension deposits and develops multiple bed morphologies, contrary to the anticipated complete suspension from the hydraulic conditions. Barchans appear on the bottom of the flume, although the total supply of silt is abundant, presumably because the availability of coarser particles capable of being deposited is limited. The bed flattens, probably as a result of the cohesive effects on the deposited silt, and a plane bed is observed for experiments that last more than two days with very high suspended sediment concentration. Van Rijn (1984) bed-load transport formula approaches bed-load transport by bedform migration, provided the critical shear velocity for initiation of motion is well defined. Ultimately, bed-load transport is several orders of

magnitude smaller than suspended transport. The segregation of the particles during the bed formation coarsens the bed, in contrast to silt remaining in suspension. Viscous effects are deemed relevant during the process of bed formation. The reasons are twofold: acting as a trap for particles and protecting the bed from erosion.

Acknowledgements

The authors thank the editors and the reviewers for their valuable comments. The authors note that there are no data sharing issues.

References

Allen, J. R. L. (1968). *Current ripples: Their relation to patterns of water and sediment motion*, North-Holland, Amsterdam, Netherlands.

Andreotti, B., Claudin, P., and Douady, S. (2002). "Selection of dune shapes and velocities part 2: A two-dimensional modelling." *Eur. Phys. J. B*, 28(3), 341–352.

Baas, J. H. (1994). "A flume study on the development and equilibrium morphology of current ripples in very fine sand." *Sedimentology*, 41(2), 185–209.

Baas, J. H. (1999). "An empirical model for the development and equilibrium morphology of current ripples in fine sand." *Sedimentology*, 46(1), 123–138.

Baas, J. H., Best, J. L., and Peakall, J. (2011). "Depositional processes, bedform development and hybrid bed formation in rapidly decelerated cohesive (mud-sand) sediment flows." *Sedimentology*, 58(7), 1953–1987.

Baas, J. H., Davies, A. G., and Malarkey, J. (2013). "Bedform development in mixed sand-mud: The contrasting role of cohesive forces in flow and bed." *Geomorphology*, 182, 19–32.

Bagnold, R. A. (1966). "An approach to the sediment transport problem from general physics." U.S. Geological Survey, Washington D. C.

Best, J. (2005). "The fluid dynamics of river dunes: A review and some future research directions." *J. Geophys. Res.*, 110, F04S02.

Boulanger, J. A. R., and Wong, C. Y. (2016). "Sand suspension deposition in horizontal low-concentration slurry pipe flows." *Granular Matter*, 18(2), 15.

Cardoso, A. H. (1998). *Hidráulica fluvial*, Fundaçao Calouste Gulbenkian, Lisboa, Portugal.

Courrech du Pont, S., Narteau, C., and Gao, X. (2014). "Two modes for dune orientation." *Geology*, 42(9), 743–746.

Endo, N., Sunamura, T., and Takimoto, H. (2005). "Barchan ripples under unidirectional water flows in the laboratory: Formation and planar morphology." *Earth Surf. Processes Landforms*, 30(13), 1675–1682.

Endo, N., Taniguchi, K., and Katsuki, A. (2004). "Observation of the whole process of interaction between barchans by flume experiments." *Geophys. Res. Lett.*, 31(12), L12503.

Folk, R. L. (1974). *Petrology of sedimentary rocks*, Hemphill Publishing, Austin TX.

Franklin, E. M., and Charru, F. (2011). "Subaqueous barchan dunes in turbulent shear flow. Part 1. Dune motion." *J. Fluid Mech.*, 675, 199-222.

Graf, W. H. (1984). *Hydraulics of sediment transport*, Water Resources, Highlands Ranch CO.

Groh, C., Rehberg, I., and Kruelle, C. A. (2009). "How attractive is a barchan dune?" *New J. Phys.*, 11(2), 023014.

Henderson, F. M. (1966). *Open channel flow*, Macmillan, New York.

Hersen, P. (2005). "Flow effects on the morphology and dynamics of aeolian and subaqueous barchan dunes." *J. Geophys. Res.*, 110(F4), F04S07.

Hersen, P., Andersen, K. H., Elbelrhiti, H., Andreotti, B., Claudin, P., and Douady, S. (2004). "Corridors of barchan dunes: Stability and size selection." *Phys. Rev. E*, 69(1), 011304.

Hersen, P., Douady, S., and Andreotti, B. (2002). "Relevant length scale of barchan dunes." *Phys. Rev. Lett.*, 89(26), 264301.

Hollister, C. D., and McCave, I. N. (1984). "Sedimentation under deep-sea storms." *Nature*, 309(5965), 220–225.

Jopling, A. V., and Forbes, D. L. (1979). "Flume study of silt transportation and deposition." *Geografiska Annaler. Series A, Phys. Geogr.*, 61(1/2), 67.

Katsuki, A., Kikuchi, M., and Endo, N. (2005). "Emergence of a barchan belt in a unidirectional flow: Experiment and numerical simulation." *J. Phys. Soc. Jpn.*, 74(3), 878–881.

Mantz, P. A. (1978). "Bedforms produced by fine, cohesionless, granular and flakey sediments under subcritical water flows." *Sedimentology*, 25(1), 83–103.

Mantz, P. A. (1992). "Cohesionless fine sediment bed forms in shallow flows." J. Hydraul. Eng., 10.1061/(ASCE)0733-9429(1992)118:5(743), 743–764.

McCave, I. N. (1970). "Deposition of fine-grained suspended sediment from tidal currents." *J. Geophys. Res.*, 75(21), 4151–4159.

McCave, I. N. (2008). "Size sorting during transport and deposition of fine sediments: Sortable silt and flow speed." *Contourites. Developments in Sedimentology*, vol. 60, Elsevier, Amsterdam, 121–142.

McCulloch, D. S., and Janda, R. J. (1964). "Subaqueous river channel barchan dunes." *J. Sediment. Petrol.*, 34(3), 694–695.

McKee, E. (1980). "A study of global sand seas." U.S. Geological Survey, Washington D. C.

Mehta, A. J. (2013). *An introduction to hydraulics of fine sediment transport*, World Scientific, Hackensack NJ.

Melo, H. P. M., Parteli, E. J. R., Andrade, J. S., and Herrmann, H. J. (2012). "Linear stability analysis of transverse dunes." *Phys. A: Stat. Mech. Appl.*, 391(20), 4606–4614.

Niño, Y., Lopez, F., and Garcia, M. (2003). "Threshold for particle entrainment into suspension." *Sedimentology*, 50(2), 247–263.

Parteli, E. J. R., Andrade, J. S., and Herrmann, H. J. (2011). "Transverse instability of dunes." *Phys. Rev. Lett.*, 107(18), 1–5.

Raudkivi, A. J. (1997). "Ripples on stream bed." *J. Hydraul. Eng.*, 10.1061/(ASCE)0733-9429(1997)123:1(58), 58–64.

Roberts, J., Jepsen, R., Gotthard, D., and Lick, W. (1998). "Effects of particle size and bulk density

on erosion of quartz particles." *J. Hydraul. Eng.*, 10.1061/(ASCE)0733-9429(1998)124:12(1261), 1261–1267.

Sauermann, G., Rognon, P., Poliakov, A., and Herrmann, H. (2000). "The shape of the barchan dunes of Southern Morocco." *Geomorphology*, 36(1–2), 47–62.

Schieber, J., Southard, J. B., Kissling, P., Rossman, B., and Ginsburg, R. (2013). "Experimental deposition of carbonate mud from moving suspensions: Importance of flocculation and implications for modern and ancient carbonate mud deposition." *J. Sediment. Res.*, 83(11), 1025–1031.

Simons, D. B., Richardson, E. V., and Nordin, C. F. (1965). "Bedload equation for ripples and dunes." U.S. Geological Survey, Washington D. C.

Southard, J. B., and Boguchwal, L. A. (1990). "Bed configuration in steady unidirectional water flows—Part 2: Synthesis of flume data." *J. Sediment. Res.*, 60(5), 658–679.

te Slaa, S., van Maren, D. S., He, Q., and Winterwerp, J. C. (2015). "Hindered settling of silt." *J. Hydraul. Eng.*, 10.1061/(ASCE)HY.1943-7900.0001038, 04015020.

van Rijn, L. C. (1984). "Sediment transport—Part I: Bed load transport." *J. Hydraul. Eng.*, 10.1061/(ASCE)0733-9429(1984)110:10(1431), 1431–1456.

van Rijn, L. C. (2007). "Unified view of sediment transport by currents 472 and waves. I: Initiation of motion, bed roughness, and bed-load transport." *J. Hydraul. Eng.*, 10.1061/(ASCE)0733-9429(2007)133:6(649), 649–667.

354 Walder, J. (2015). "Dimensionless Erosion Laws for Cohesive Sediment." *J. Hydraul. Eng.*,
355 10.1061/(ASCE)HY.1943-7900.0001068, 04015047.

356 Zhang, D., Yang, X., Rozier, O., and Narteau, C. (2014). "Mean sediment residence time in
357 barchan dunes." *J. Geophys. Res. Earth Surf.*, 119(3), 451–463.

358

Publisher version: doi: 10.1061/(ASCE)HY.1943-7900.0001212

359 Table 1. Silt concentration and silt bed morphology

Code	t (min)	C_0 (kg/m^3)	C_f (kg/m^3)	n	N	W (cm)	L (cm)	H (cm)	H_{max} (cm)	L_h (cm)	λ (cm)	vol. (cm^3)	s (cm)
							Group 1						
E1	100	7.51	6.81	900	0.36	4.48	6.13	0.35	0.51	-	8.98	3.20	0.00
E2	100	21.30	19.22	900	0.40	4.84	6.31	0.38	0.50	-	9.14	3.87	0.05
							Group 2						
E3	1440	1.28	0.87	200	0.11	4.24	9.00	0.37	0.53	1.47	-	4.89	0.00
E4	1440	1.99	1.30	250	0.19	4.87	10.40	0.39	0.53	1.54	-	6.82	0.00
E5	1440	3.01	2.00	250	0.22	5.24	11.29	0.37	0.62	1.53	-	7.53	0.02
E6	1440	3.57	2.18	250	0.18	4.79	10.14	0.41	0.62	1.29	-	6.84	0.05
E7	1440	4.44	2.96	220	0.13	4.19	8.98	0.33	0.56	1.25	-	4.28	0.08
E8	1440	4.52	3.02	220	0.12	4.37	9.48	0.34	0.56	1.26	-	4.84	0.08
E9	1440	9.17	6.42	450	0.43	5.59	11.73	0.67	0.79	1.55	17.35	15.10	0.04
E10	1440	9.82	7.09	500	0.52	6.11	11.65	0.69	0.83	1.31	15.94	16.81	0.00
							Group 3						
E11	4320	22.46	11.95	-	-	-	-	-	1.17	-	-	-	0.70
E12	2040	51.72	33.04	-	-	-	-	-	2.26	-	-	-	1.25

360 Note: C_0 = initial and C_f = final suspended sediment concentration. Measurements relate to a single
361 bedform of average dimensions; n = approximate total number of bedforms on the entire floor of
362 the flume; N = ratio of area of flume bottom with barchans to total area of flume bottom where the
363 area of one barchan is evaluated as the area enclosed by an ellipse (stoss-side) and a parabola
364 (toeline); W = width between horns, L = body length, H = height, L_h = horn length H_{max} =
365 maximum bedform height in cm; λ = distance between consecutive barchans fronts; vol. = volume
366 of a barchan (cm^3), evaluated by slicing the barchan in triangles defined by an ellipse and a
367 parabola (they define the base of the triangle) and the height, which is related to the base through
368 invariant lee-side and the stoss-side angles; s = thickness (cm) of a plane layer that covers the
369 whole flume bed on top of which the ripples are an addition [Fig. 5(c)]. Average standard

370 deviations of the measures of width, length, height and horn length are 1.14 cm, 2.17 cm, 0.13 cm

371 and 0.53 cm, respectively.

372

373 Table 2. Silt bed grain size

Silt bed	*Initial*	*Group 1*	*Group 2*	*Group 3*
D_{10} (μm)	1.25	2.49	1.96	1.80
D_{50} (μm)	4.37	11.17	9.78	21.14
D_{90} (μm)	12.48	25.33	23.24	7.95
D_g (μm)	4.15	9.35	7.97	6.78
σ_g (-)	2.38	2.48	2.78	2.73

374 Note: D_x = size for which x % of the sample is finer. Initial grain size relates to sediment in
375 suspension at the beginning of the experiments.
376
377 List of Figures

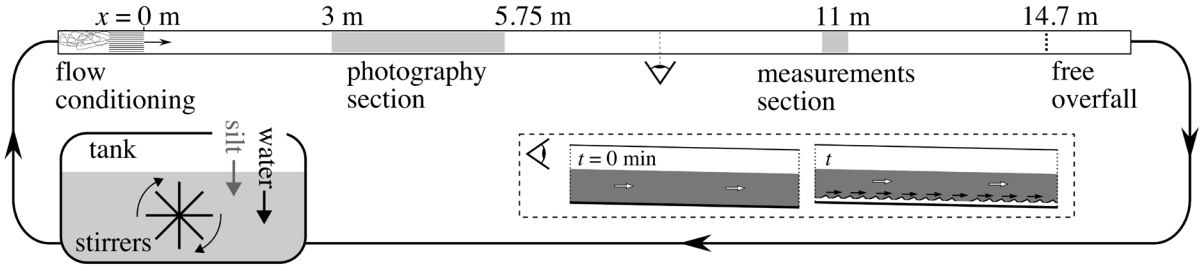

378

379 Fig. 1. Schematic drawings of the experiments.

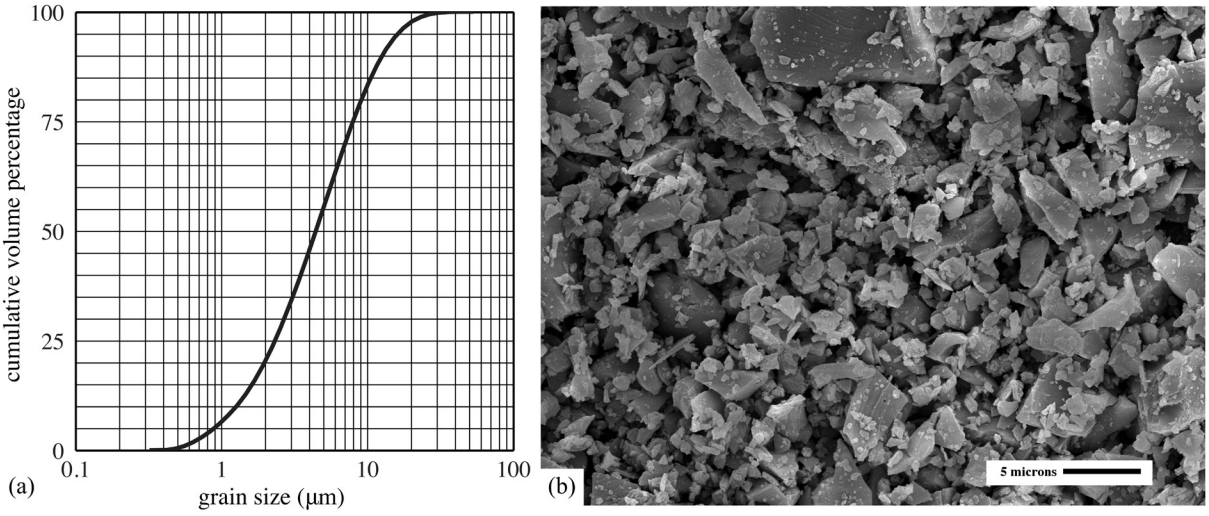

380

Publisher version: doi: 10.1061/(ASCE)HY.1943-7900.0001212

381 Fig. 2. (a) Cumulative size distribution of the quartz silt; (b) high-resolution image of the particles.

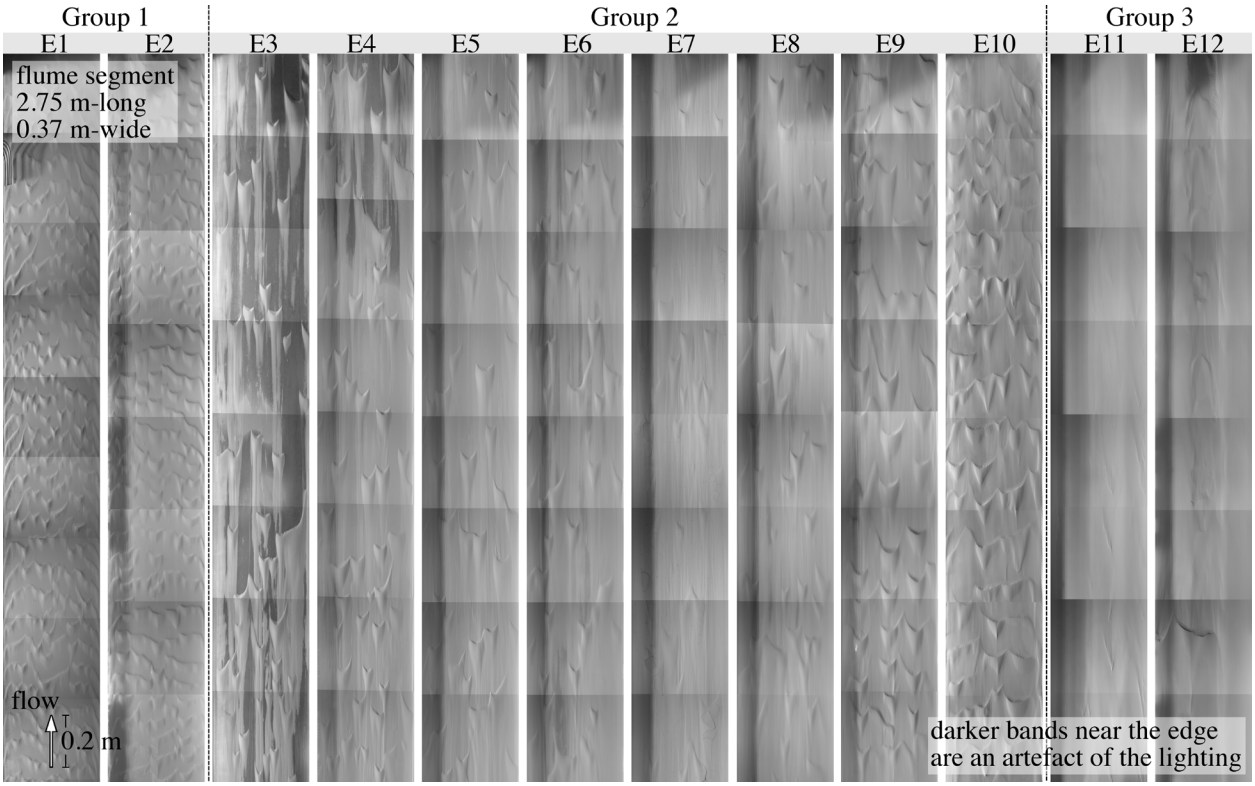

382

383 Fig. 3. Beds of quartz silt at the end of the experiments.

Publisher version: doi: 10.1061/(ASCE)HY.1943-7900.0001212

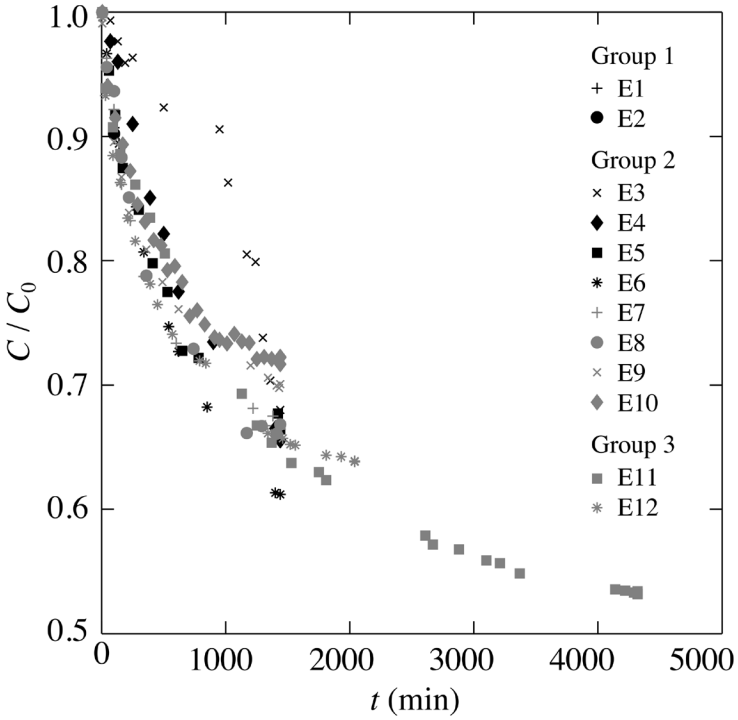

384

385 Fig. 4. Decrease in relative concentration over time.

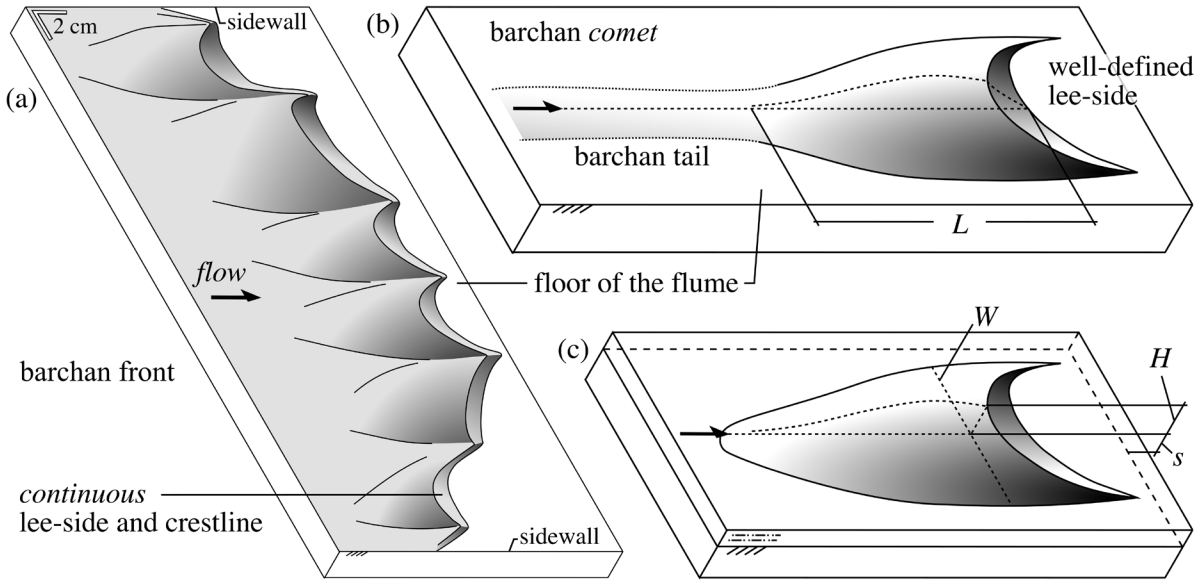

386

387 Fig. 5. Quartz silt bed elements: (a) barchan front; (b) barchan comet; (c) barchan emerging from

388 a silt layer